



Forensic Anthropology

Suitability of 3D printing cranial trauma: Prospective novel applications and limitations of 3D replicas

Rachael M. Carew^{a,b,*}, James French^{a,b}, Ruth M. Morgan^{a,b}

^a UCL Department of Security and Crime Science, 35 Tavistock Square, London WC1H 9EZ, UK

^b UCL Centre for the Forensic Sciences, 35 Tavistock Square, London WC1H 9EZ, UK



ARTICLE INFO

Keywords:

Forensic anthropology
3D imaging
3D modelling
3D printing
Evidence reconstruction
Trauma

ABSTRACT

3D printed reconstructions of skeletal material offer a novel, interactive and increasingly used tool to support courtroom testimony and aid juror interpretation of expert testimony. While research has begun to address the accuracy of 3D printed skeletal material, there has been little consideration of the diverse applications of prints to support trauma demonstrations, particularly in relation to gunshot trauma. This study explored the suitability of three printed human crania replicas exhibiting either gunshot trauma or blunt force trauma for identifying whether the prints were sufficiently accurate for the presentation of trauma wounds. The data indicate that metric measurement and qualitative assessment of trauma macromorphology was possible from the 3D printed reconstructions. The findings also offer an indication that it is possible to obtain data around the accuracy of 3D printing bullet wounds and for establishing a bullet path. However, some limitations of prints reconstructed from post-mortem computed tomography (PMCT) data were identified including the observation that not all fracture lines were successfully replicated which indicates that at present virtual models should be used concurrently with 3D prints in court.

1. Introduction

Recording and demonstrating peri-mortem skeletal trauma is an important aspect of medico-legal investigations [1]. Through the analysis of peri-mortem skeletal injuries, a forensic specialist (e.g. a forensic anthropologist, pathologist, or radiographer) can ascertain important intelligence to inform an indication of the cause of death of an individual, as well as the mechanism of death or the mode of body disposal [2]. These findings may also be presented to a court of law, where the consideration of potentially graphic, confrontational evidence needs to be carefully considered for its prejudicial impact and admissibility requirements [3]. In this context, using demonstrative visual aids can be valuable as a means of presenting evidence of skeletal injuries in a less-confrontational manner [4,5]. Research has shown that 3D printed skeletal reconstructions can offer a useful visual aid that can help lay members of the court to better understand expert testimony [4,5]. However, it is important that novel techniques, such as 3D printed reconstructions, are researched using empirical data to show that prints are demonstrably accurate and underpinned using an evidence-base to help avoid misinterpretation and misrepresentation of evidence in

courts of law [6,7]. This study therefore investigates the suitability of novel three-dimensional (3D) printed trauma models for potential investigative or courtroom demonstration purposes, to begin to explore the applications of 3D printed trauma wounds for forensic applications.

There are three classifications of trauma, sharp force trauma (SFT), blunt force trauma (BFT), and ballistic trauma (or gunshot trauma, GST) [8]. BFT is the most common form of injury examined by forensic practitioners [8,9] and can generally be identified by the presence of an impact area, combined with (some or all of) radiating and concentric fractures, delamination of bone, plastic deformation and internal beveling [8]. Methodical analysis of trauma sites can lead to assessment of the impact sites, the number and sequence of impacts, and potentially tool classification [8]. However, trauma interpretation can be complicated by factors such as the age, sex and health of the individual as well as the impact angle, mechanism and force exerted, in addition to the presence, and type, of clothing [9]. With GST, forensic scientists may ascertain information regarding the direction and orientation of the bullet trajectory and the sequence of impacts, the length of distance travelled by the bullet and the calibre of the bullet [8,10–12]. Henwood et al. [11] found that they could distinguish between bullet wounds

* Corresponding author at: UCL Department of Security and Crime Science, 35 Tavistock Square, London WC1H 9EZ, UK.

E-mail addresses: rachael.carew.16@ucl.ac.uk (R.M. Carew), james.french@ucl.ac.uk (J. French), ruth.morgan@ucl.ac.uk (R.M. Morgan).

<https://doi.org/10.1016/j.fsir.2021.100218>

Received 11 February 2021; Received in revised form 11 June 2021; Accepted 1 July 2021

Available online 3 July 2021

2665-9107/© 2021 The Authors. Published by Elsevier B.V. This is an open access article under the CC BY license (<http://creativecommons.org/licenses/by/4.0/>).

made from .22 calibre bullets (5.6 mm) with those made by .38 calibre bullets (9 mm) using metric assessment, and Marais and Dicks [12] performed metric assessment via computed tomography (CT) scanning to exclude a suspected bullet from a forensic investigation. Carew and Errickson [13] have also suggested the potential for using 3D printed replicas to establish bullet pathways given that entry and exit GST wounds can present features indicative of the path of a bullet through an object, which can aid the determination of further intelligence, such as the position of gunshot residue or in calculating positions of the different actors involved in the forensic event [10,14]. While estimating bullet calibre from a GST may be possible, there is not always a straightforward relationship between the wound size and bullet size as it is complicated by the size, direction and speed of the bullet, as well as the complexity introduced by bone biomechanics [8].

Post-mortem computed tomography (PMCT) scanning has been increasingly used in forensic anthropology [14–17] to assist the visualisation, interpretation and recording of skeletal injuries as it is non-invasive and can be undertaken without direct contact [2,3,16]. This non-invasive method also offers an approach that is more ethical than maceration procedures and can for example provide an approach that is more suitable for religions that are opposed to traditional invasive autopsy [18]. Three-dimensional (3D) reconstructions from PMCT data can provide a visualisation of peri-mortem injuries for the interpretation of injuries and forensic events as well as for courtroom demonstrations [19–21], with the quality of the reconstruction being dependent on the CT acquisition and 3D modelling parameters, and observer experience [3,17]. Published research has demonstrated that printed replicas can be sufficiently accurate for demonstrative purposes of gross morphological features to around 1–2 mm [6,22,23], but with some limitations of the display of fine surface features [22] including the conclusion of fracture lines [23].

Effective presentation of skeletal trauma in a courtroom can be challenging since post-mortem photos often cannot be shown in courtrooms in the UK as they are considered to be too graphic and overly prejudicial towards the prosecution [24,25], however, 3D virtual models and 3D printed replicas generated from PMCT scan data offer alternative visualisation formats that are less graphic and potentially less prejudicial [4,25]. Recent research has demonstrated that jurors may better understand expert testimony when presented with 3D printed visual aids rather than when alongside photographs [4,5]. The primary advantage of having a 3D printed replica, is the provision of a physical replica that a juror can hold, touch, rotate, and even use to mimic injuries [26]. The 3D print adds an additional level of spatial and haptic processing information that can aid the juror in their interpretation of the courtroom testimony. Further, the benefits of utilising 3D prints in forensic science were discussed by Carew and Errickson [13], in forensic odontology by Jani et al. [27] and in forensic medicine by Schweitzer et al. [28]. Nevertheless, despite the potential for 3D printing physical replica models, most PMCT reconstructions of peri-mortem trauma remain presented stereoscopically on two-dimensional screens [14]. Further exploration of the use and application of 3D printed visual aids could help demonstrate the benefits but also identify potential limitations, and ultimately help forensic scientists to decide whether to invest in producing 3D printed reconstructions.

Utilising 3D printing for trauma analysis of human remains has been demonstrated for several applications, including for cranial BFT and weapon identification [20,29,30], for SFT toolmark analysis on ribs [31], toolmark and physical fit analysis of a humerus [29] and physical fit analysis of burnt long bone fragments [32]. However, no published literature has been identified that has investigated the application of 3D printed replica human bones exhibiting GST in forensic anthropology contexts. This study assesses the potential applications of 3D printing cranial trauma focussing on one case of BFT and two cases of GST by exploring whether 3D printed replica human bones could be suitable for trauma reconstructions, including representation of bullet wound size and demonstration of bullet paths. To explore the suitability of 3D

printing cranial trauma, this study assesses the degree to which it is possible to:

- 1) accurately measure trauma wounds from a print compared with a virtual model
- 2) demonstrate a bullet path through a printed cranium exhibiting GST
- 3) visualise GST and BFT effectively on a print

2. Materials and methods

2.1. Materials

Three forensic case samples were obtained from a clinical casework data collection. This included two dry human (*Homo sapiens*) bone samples, and one PMCT scan (Digital Imaging and Communications in Medicine (DICOM) data). Case 1 was a dry bone calvarium exhibiting GST, with entry and exit holes on the left and right parietal bones respectively (Fig. 1). Case 2 was a dry bone calvarium exhibiting BFT with concentric and radiating fractures on the left parietal bone and plastic deformation on the ectocranial surface (Fig. 1). Case 3 was PMCT DICOM data of an adult female exhibiting cranial GST, with an entry wound on the right parietal bone and an exit wound on the left temporal bone combined with bone flaking and radiating fractures (Fig. 2).

All scan data was acquired using a Siemens Emotion 6 CT scanner; cases 1 and 2 (dry bone calvaria) were scanned by a clinical CT radiographer scanned using parameters chosen from their own knowledge. Scan parameters were 0.63 mm slice thickness, 130 kVp, data collection diameter 500 mm, Xray tube current 158, 166 (case 1 and 2 respectively) and reconstruction diameter 194 mm, 210 mm (case 1 and 2 respectively), pixel spacing 0.37 mm and 0.41 mm with reconstruction/convolution kernel H90s. Case 3 (the PMCT data) was scanned previously as part of a clinical PM examination. Scanning parameters for case 3 were 0.63 mm slice thickness, 130 kVp, data collection diameter 500 mm, Xray tube current 82 and reconstruction diameter 227 mm, pixel spacing 0.44 mm with reconstruction/convolution kernel H20s. The CT images were all saved as Digital Imaging and Communications in Medicine (DICOM) data and were viewed using the open-source software 3D Slicer (Brigham Women's Hospital, Boston, MA, US) [33,34].

The method for generating a 3D surface model from the DICOM data followed the tested method presented in Robles et al. [35]. The region of interest was cropped from any surrounding material and semi-automatic thresholding was used to segment the skeletal material based on the HU threshold values. The PMCT data required additional manual segmentation steps to remove any adjacent material such as the cervical vertebrae (as can be seen in the 2D multiplanar reconstructions in Fig. 2). The 3D surface models were exported as STL (stereolithographic) files (Fig. 3), postprocessed in Blender (Stichting Blender Foundation, Amsterdam, the Netherlands) [36], and smoothed by a factor of 0.5 (iterated ten times) using the Smooth Modifier tool. The smoothing and 3D printing steps followed the recommendations set out by Carew et al. [6] for generating accurate 3D printed bone reconstructions. The STL files were all printed using an EOSINT P100 selective laser sintering (SLS) printer (EOS GmbH Electro Optical Systems, Germany) at 100 µm layers (0.1 mm). SLS is a powder bed fusion method utilising a white powder-based material (PA2200, nylon 12).

2.2. Experimental Investigation

2.2.1. Metric assessment

A series of linear metric measurement points on each sample were chosen to ascertain the overall dimensions of each trauma wound (Table 1). These included the maximum and minimum diameters of the lesions and length of fracture lines since the lesions are not uniform but irregular in shape. Comparisons were performed between the virtual models and the 3D prints since the original skeletal material was no longer available (for cases 1 and 2) and to represent cases where



Fig. 1. Differing views and trauma features exhibited on case 1 and case 2 dry bones. Upper left: case 1 left lateral view with GST entry wound; upper right: case 1 right lateral view with GST exit wound and external bevelling (star); lower right: case 2 inferior view of ectocranial surface with plastic deformation; lower left: case 2 left lateral view of BFT with radiating, and concentric fractures (arrows).

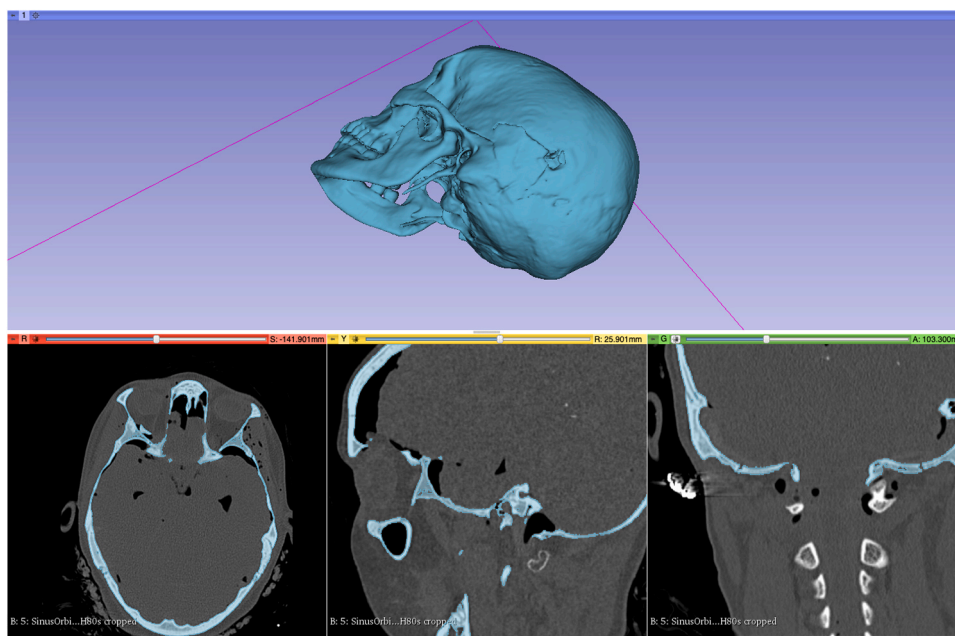


Fig. 2. Views of case 3 PMCT DICOM segmentation showing left lateral posterior-inferior view of 3D model (upper) and 2D multiplanar reconstructions (lower); screenshots taken with 3D Slicer.

invasive autopsy examination is avoided. A total of 16 measurements were taken twice each by two observers, in a similar manner to the protocol outlined by Carew et al. [22]. Taking several measurements from each lesion reduced the chance of anomalous data affecting the results. In addition, the introduction of an inter-observer comparison was included to minimise observer bias. The measurement data were obtained from the 3D printed replicas using digital sliding calipers (to the nearest millimetre). The measurements were then recorded from the

corresponding virtual 3D models (STL files) in 3D Slicer using the Ruler tool (to the nearest millimetre). The observers were a forensic anthropologist and an aerospace engineer, both experienced at taking measurement data from virtual computer models and physical models, with 5 years and over 10 years of experience respectively. The repeated measurements were recorded over two separate days for both the printed and virtual models (four days total), to minimise the risk of context or familiarity influencing the measurements. The resulting

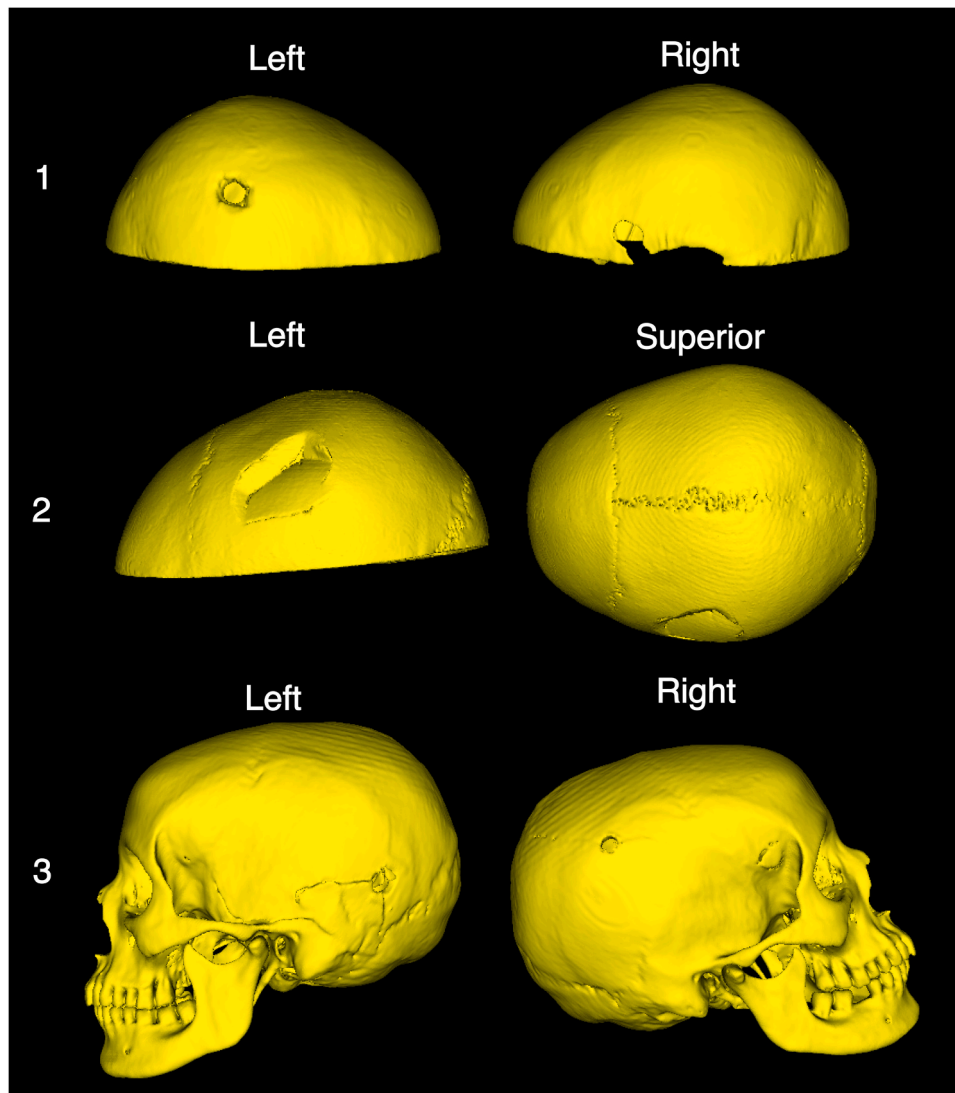


Fig. 3. Views of the 3D models (STL files) from the three cases (1–3); viewed as screenshots taken in 3D Slicer.

measurement data was converted into a percentage difference (by dividing the difference value (mm) by the virtual mean (mm)) to provide a non-dimensionalised value that is independent of the size of the measured feature [37,38].

The repeatability of the inter-observer measurement data was tested by considering the variance and within-subject standard deviation (wSD; square root of the average variances) as previously used [6,39]. The mean measurement data taken from the virtual and the 3D print models were then compared using a two-tailed paired *t*-test (with significance of 0.05) to identify any potential significance in measurement variability. To assess accuracy, an ideal threshold of ± 1.0 mm was used as the cut-off point (as suggested by Carew et al. [22]), as well as a percentage cut-off value of 3% [38].

2.2.2. Identifying bullet paths

The entry and exit GST wounds on case 1 were used to infer the path of the injury causing bullet. The bullet wounds were aligned on the 3D model, and a computer modelled rod was generated using Blender to demonstrate the path of the bullet through the entry and exit wounds. The STL file including both the calvarium and the rod was then exported for viewing in 3D Slicer to obtain a visualisation in anatomical orientation. The STL file was then 3D printed using a desktop Flashforge filament deposition (FDM) printer. The file was printed to a 30% scale,

to enable it to fit inside the printer and to ensure the print could be completed in a timely manner (approximately 3.5 h). A ‘hyper’ resolution print was selected using the Flashprint software (layer height 0.08 mm) that included tree supports and a build raft, with a white PLA filament material. The external tree supports and raft were manually removed after printing.

2.2.3. Qualitative comparison of macromorphoscopic trauma features

Photographs of the original calvaria bones (cases 1 and 2) were compared with the printed replica calvaria to assess the quality of the prints, by visually searching for any similarities and differences in the representation of macromorphoscopic trauma features on the prints, following the procedure outlined by Carew et al. [22].

For the PMCT cranium (case 3), volume renderings of the original CT data were compared with the printed replica cranium, to assess the quality of the printed cranium and the representation of macromorphoscopic trauma features on the prints and to identify any similarities and differences in the same way as for cases 1 and 2.

Table 1
Data collection measurement points recorded on samples A-C.

Case	Feature	Measurement Point
1	Exit wound (complete circular defect on external surface)	1 Maximum inner diameter
	Exit wound (complete circular defect on external surface)	2 Maximum outer diameter
	Entry wound (incomplete circular defect on external surface)	3 Maximum length of wound
	Entry wound (incomplete circular defect on external surface)	4 Minimum internal diameter of wound
	Entry wound (incomplete circular defect on external surface)	5 Maximum internal diameter of wound
2	Trauma wound (external surface)	6 Length of inner fracture line
	Trauma wound (external surface)	7 Length of outer fracture area
	Trauma wound (external surface)	8 Maximum width of outer fracture area
	Trauma wound (internal surface)	9 Length of inner fracture line
	Trauma wound (internal surface)	10 Length of outer fracture area
3	Trauma wound (internal surface)	11 Maximum width of outer fracture area
	Trauma wound (right side of skull)	12 Minimum diameter of wound
	Trauma wound (right side of skull)	13 Maximum diameter of wound
	Trauma wound (left side of skull)	14 Minimum diameter of wound
	Trauma wound (left side of skull)	15 Maximum diameter of wound
	Trauma wound (left side of skull)	16 Length of large fracture line

3. Results

3.1. Metric assessment

The measurement data obtained by observers 1 and 2 (Table 2) were explored to assess the accuracy of the trauma wound measurement from a print compared with the measurement from the virtual model (Table 3).

Repeatability analysis of measurement data from observer 1 resulted in overall wSD values of 0.6 mm (1.7 mm 95% repeatability) for the 3D print data, and 0.1 mm (0.2 mm 95% repeatability) for the virtual model data. The data for observer 2 resulted in overall wSD values of 0.4 mm (1.1 mm 95% repeatability) for the 3D print data, and 0.1 mm (0.3 mm 95% repeatability) for the virtual model data.

The differences between the 3D print and virtual measurement data

Table 2

Virtual and 3D print measurement data recorded by observer 1 and 2 (taken twice each) for each measurement point on the three crania (case 1–3).

Case	Measurement Point		Print Measurement (mm)				Virtual Measurement (mm)			
			Obs1_1	Obs1_2	Obs2_1	Obs2_2	Obs1_1	Obs1_2	Obs2_1	Obs2_2
1	1	Maximum inner diameter	10.4	10.9	10.4	10.4	10.7	10.6	10.6	10.3
	2	Maximum outer diameter	19.3	20.2	19.5	19.1	19.5	19.8	20.3	19.8
	3	Maximum length of wound	20.0	20.5	20.7	20.8	19.8	19.9	20.3	20.1
	4	Minimum internal diameter of wound	10.4	10.3	10.6	10.7	8.6	8.6	11.1	11.3
	5	Maximum internal diameter of wound	13.7	14.2	13.8	13.8	14.3	14.2	15.0	15.0
2	6	Length of inner fracture line	29.6	29.8	29.6	29.1	31.4	30.9	29.7	30.3
	7	Length of outer fracture area	56.4	54.6	53.2	53.7	50.1	52.7	53.9	54.7
	8	Maximum width of outer fracture area	35.5	39.1	39.5	39.0	37.8	37.7	38.5	38.0
	9	Length of inner fracture line	41.3	42.0	41.4	41.6	37.1	38.5	38.4	37.4
	10	Length of outer fracture area	49.9	50.2	50.1	50.0	48.5	48.9	51.5	51.1
	11	Maximum width of outer fracture area	36.2	35.9	36.6	36.6	37.2	37.5	37.8	38.0
3	12	Minimum diameter of wound	6.7	7.4	7.7	7.2	8.6	8.1	6.3	6.3
	13	Maximum diameter of wound	7.5	7.2	7.2	7.6	8.7	8.4	8.0	8.2
	14	Minimum diameter of wound	8.6	7.8	7.6	7.6	10.3	9.2	8.2	8.5
	15	Maximum diameter of wound	7.9	7.9	8.8	8.0	11.3	10.3	11.0	11.0
	16	Length of large fracture line	35.2	35.1	36.5	36.5	35.8	34.9	36.5	36.2

ranged from -2.8 – 3.7 mm. The accuracy of the 3D printed cranium from case 1 was within the ± 1.0 mm threshold for all measurement points (Table 3). Several of the measurement points for cases 2 and 3 were above the accuracy threshold level. There was no statistical significance observed between the mean print and virtual data (p-value 0.8). The percentage difference of the accuracy data ranged from -25 – 10% , with a mean difference of -3% .

3.2. Demonstrating bullet paths

From the 3D virtual models, it was possible to see the inferred path of the bullet through the calvarium and how the entry and exit wounds aligned (Fig. 4). It was also possible to alter the colour of the models and background, add in positional aids (such as the homunculus) and orient the models into anatomical position for further views. This assisted the development of the 3D models into visual aids that were both visually engaging and demonstrated anatomical accuracy by orienting the observer. Additionally, the software allows the recording of videos, such as of the model rotating through 360° , which created a visual aid for demonstration purposes that demonstrates a full view of the sample or injury from different aspects.

The STL model was 3D printed using FDM to demonstrate the potential for a 3D print to assist with the identification of the bullet trajectory (Fig. 5). The 3D model was successfully produced as a 3D print, which demonstrated the path of the bullet through the calvarium with the printed rod in place. The print was a small size (approximately 4×5 cm, excluding the rod [see scale in Fig. 5]) that was robust and easy to hold and could easily be passed between individual observers. However, the quality of this FDM print was poor, with scan lines visible on the surface and rough edges present after removing the support structures. The computer modelled rod was held in place with supports that obscured the GST entry and exit wounds.

3.3. Qualitative comparison of macromorphoscopic trauma features

The macromorphological features on the two dry calvaria (case 1 and 2) (Fig. 1), were subsequently observed on the SLS 3D printed replica calvaria (Fig. 6). The entry and exit GST wounds on case 1 were effectively visualised on the printed replica, with the wounds, or holes, being successfully printed with no visible inclusion of material. The wounds were surrounded by clear boundaries that marked a change in bony structure and included external and internal bevelling, although there was some loss of detail with the porosity and microfractures radiating away from the external bevelling. The BFT trauma macromorphological features on case 2 were also effectively visualised on both the endocranial and ectocranial surfaces of the printed replica, where the plastic

Table 3

Differences between mean measurements for the 3D print and virtual models as a percentage difference (mean print value minus mean virtual value) (mm). * indicates value outside of the accuracy range $\geq \pm 1.0$ mm, or percentage cut-off $> 3\%$.

Case	Measurement Point	3D Print Mean (mm)	Virtual Mean (mm)	Difference (mm)	Percentage difference
1	1 Maximum inner diameter	10.5	10.6	0.0	0%
	2 Maximum outer diameter	19.5	19.9	-0.3	-2%
	3 Maximum length of wound	20.5	20.0	0.5	2%
	4 Minimum internal diameter of wound	10.5	9.9	0.6	6%*
	5 Maximum internal diameter of wound	13.9	14.6	-0.8	-5%*
2	6 Length of inner fracture line	29.5	30.6	-1.1*	-3%*
	7 Length of outer fracture area	54.5	52.9	1.6*	3%*
	8 Maximum width of outer fracture area	38.3	38.0	0.3	1%
	9 Length of inner fracture line	41.6	37.9	3.7*	10%*
	10 Length of outer fracture area	50.1	50.0	0.0	0%
	11 Maximum width of outer fracture area	36.3	37.6	-1.3*	-3%
3	12 Minimum diameter of wound	7.3	7.3	-0.1	-1%
	13 Maximum diameter of wound	7.4	8.3	-0.9	-11%*
	14 Minimum diameter of wound	7.9	9.1	-1.2*	-13%*
	15 Maximum diameter of wound	8.2	10.9	-2.8*	-25%*
	16 Length of large fracture line	35.8	35.9	0.0	0%

deformation and fracture lines were observable, except for the loss of microfractures on the print (Fig. 6).

A qualitative comparison of trauma features on case 3 initially showed good resemblance between the STL 3D models (Fig. 3) and the 3D printed replica skull (Fig. 7). When visually examining the surface of the print, good congruence was found with the radiating fracture lines anterior and inferior to the gunshot exit wound on the left parietal bone, with these features seen on the STL 3D model clearly visible on the 3D print. Small bone fragments were also identified as still in-situ on the external surface of the exit wound on the model and print (Fig. 7). To ensure that these in-situ fragments were true bony features, rather than scan or print artefacts, the volume renderings from the original PMCT data were re-examined and confirmed to be bony fragments. Further

congruence between the volume rendering and the printed replica was checked and subsequently, a number of fractures lines were identified that were absent (or not strongly presented) in the STL 3D model or the 3D printed replica (Fig. 7). In particular, there were two large radiating fractures that started at the entry wound on the right parietal bone and radiated (one anteriorly and one posteriorly) across the cranium and terminated at the exit wound on the left parietal bone, which were largely absent on the STL models and subsequent prints.

4. Discussion

This research explored the suitability of novel three-dimensional (3D) printed trauma models for the purpose of presenting trauma features in a courtroom demonstration as a visual aid. Three case examples of 3D printed crania exhibiting BFT and GST were presented and the degree of congruence between the prints and the original samples was examined to assess the degree to which 3D prints could be used to convey key findings in expert testimony to a lay audience, such as a jury.

4.1. Metric assessment

A comparison of linear metric measurement data taken from the trauma features on printed replicas and 3D models was undertaken to identify whether the trauma features on the prints were consistent with comparable measurements from the virtual 3D models. Statistical analysis indicated good repeatability between the measurements achieved by two observers, with low wSD and repeatability values. The accuracy of the 3D prints compared with the virtual models was within a threshold of ± 1.0 mm for the majority of the measurement points, with all points from case 1 meeting this standard (Table 3). However, given the size of the features being measured (as small as 7.0 mm), it may be more appropriate to report findings using the non-dimensionalised percentage values and using a percentage cut-off value rather than the previously reported ± 1.0 mm cut-off. The percentage cut-off value of 3% discussed by Baier et al. [38] was used, which resulted in three additional values being considered as 'outside' of the percentage cut-off value (Table 3, measurement points 4, 5 and 13). When measuring features of a small size, such as the GST wound diameters in this study, and the toolmarks measured by Baier et al. [38], various factors such as the level of precision used and observer measurement error need to be considered to develop a cut-off threshold that is practicable when measuring to such small degrees.

Discrepancy in the accuracy measurements could be due to inter-observer differences in the measurement data, which can be attributed to the ambiguity of the point descriptions. For example, measurement point 9 for case 2 was difficult to determine as the fractured surface was not linear, similarly, measurement point 9 on case 3 was difficult to access with the sliding calipers due to the in-situ bone fragments obscuring the exit wound. The measurement points selected were not for measuring trauma features nor were they standard measurement points, such as the craniometric measurement points used for sex estimations, as these would not have been appropriate for measuring a calvarium. The wide ranging non-dimensionalised percentage values demonstrate the variability in accuracy values obtained. Going forward it may be necessary to develop a rationale for measurements that are appropriate for cranial trauma wounds with a narrower margin for measurement error and developing a percentage accuracy threshold as has been discussed [37,38]. Nevertheless, there was no statistically significant difference observed between the 3D print and virtual model data indicating that the 3D prints offered sufficiently metrically accurate representations of the virtual models.

This metric assessment provided a method to assess the accuracy of the trauma features on the 3D printed bones. Such an assessment can be performed in casework and the degree of accuracy could be disclosed to the court as evidence of the accuracy and reliability of the reconstruction. By declaring the level of accuracy to the court, an expert can

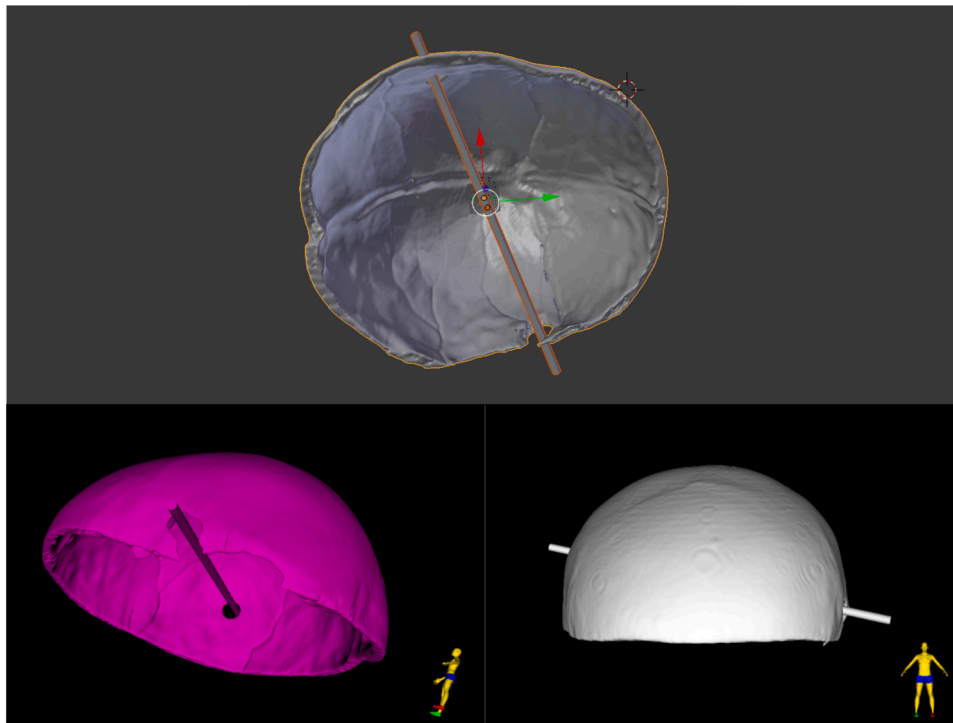


Fig. 4. Demonstration of the path of a bullet through the entry and exit wounds on the calvarium with a computer modelled rod (case 1). Top: inferior view in Blender; lower left; left lateral view in 3D Slicer; lower right: anterior view in 3D Slicer.

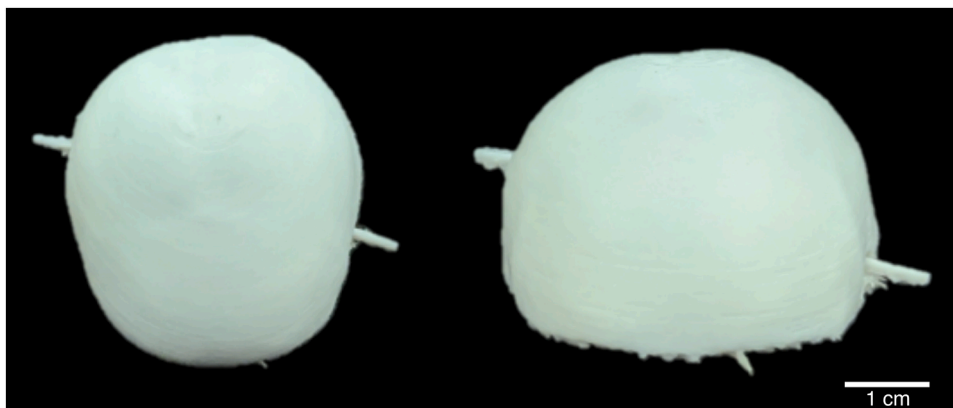


Fig. 5. Photographs of 3D printed case 1 with rod demonstrating bullet path (30% scale model).

demonstrate that they are acting transparently. Further, the accuracy of the visual aid can better withstand admissibility criteria or cross-examination and may also be entered as substantive evidence if required.

4.2. Demonstrating bullet paths

The bullet path was successfully visualised through the virtual calvarium by using the computer-generated rod to illustrate the direction of travel between the GST entry and exit wounds. The inclusion of colour provided visually appealing models, something that may aid in making the model less-graphically disturbing and more acceptable for courtroom use, as demonstrated by Villa et al. [40]. The addition of an arrow could also provide additional information depicting the direction of travel of the bullet, this combined with the alignment of the entry wound gives information about the incident. For example, given that the entrance GST wound aligns with the GST exit wound via the endocranial vault, with no other GST wounds visible, indicates that the entry and exit

wound align. This alignment combined with the direction of bullet travel indicates that the two wounds were caused by one GST act with a bullet that travelled completely through the cranium in one particular direction. The virtual model was a straightforward visualisation tool to demonstrate the path of the bullet in virtual space, similar to the findings by Puentes et al. [10] who successfully visualised a bullet path present in a lower limb using PMCT models. The 3D printed version demonstrating the bullet path also showed the potential for printing bullet paths as visual aids, providing a simple, affordable, physical model, although the scale and quality used in this study appeared poor, the resolution of the FDM printer was greater than the SLS printer. Moreover, improved quality may be obtained using a different printer, with the supports printed in a different colour, or at full scale to produce a replica with better aesthetics (which was unavailable in this study due to time and cost restraints). The use of scaled replicas in a courtroom would need to be carefully considered to ensure the court understands the associated changes to scale.

The 3D models and 3D prints assessed in this study created virtual

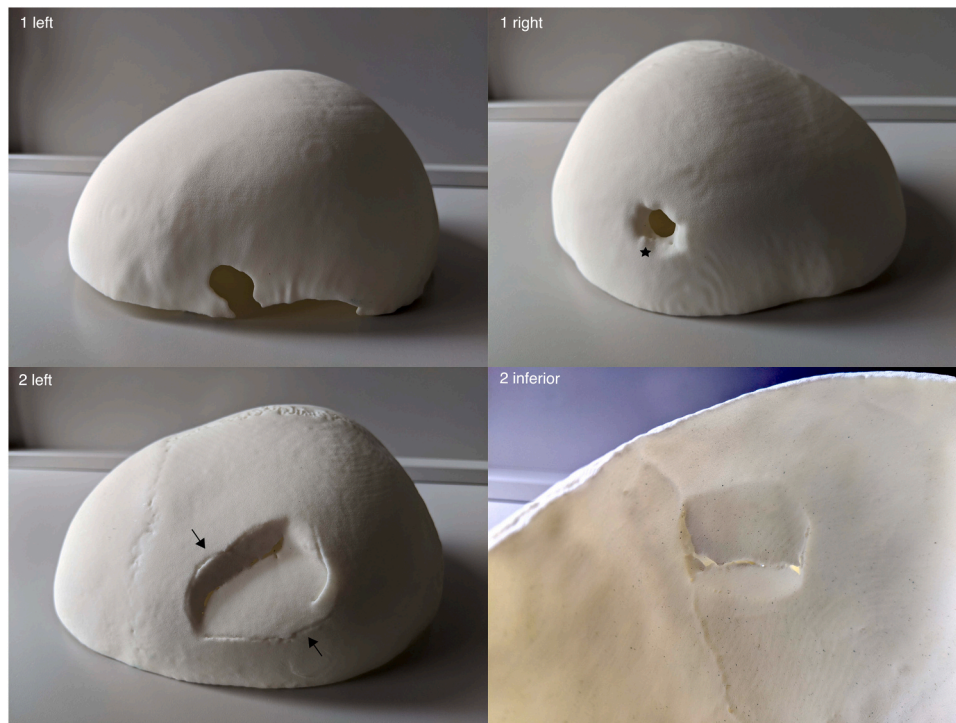


Fig. 6. Differing views and trauma features exhibited on case 1 and case 2 SLS 3D printed replicas. Upper left: case 1 left lateral view with GST entry wound; upper right: case 1 right lateral view with GST exit wound and external beveling (star); lower right: case 2 inferior view of ectocranial surface with plastic deformation; lower left: case 2 left lateral view of BFT with radiating, and concentric fractures (arrows).

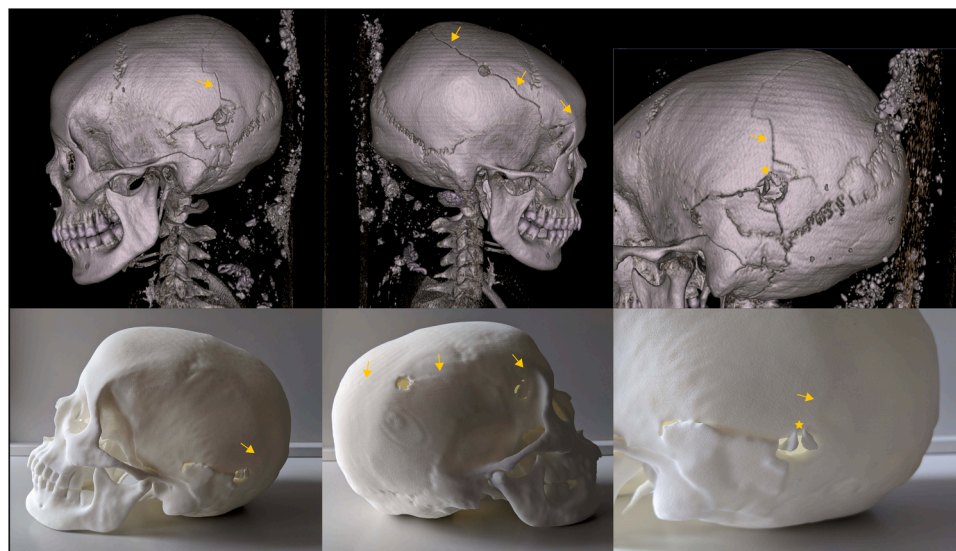


Fig. 7. Cranium (case 3) volume renders from PMCT data (upper images) and SLS 3D printed replica cranium (lower images). Left lateral view (left), right lateral view (centre) and close-up left lateral view (right). Arrows illustrating position of radiating fractures (absent in prints); star illustrating small fragments in-situ.

tools that appear to be clear and easy to interact with as well as being tangible physical tools. These two attributes combined with the results from the metric assessment, indicate that there is potential for these models to be used as visual aids for demonstrating bullet path evidence as previously suggested by Carew and Errickson [13]. Currently, it is not known to what extent factors such as the inclusion of colour, model annotation, or scaled prints has on the understanding and evaluative interpretation of visual aids like these in a courtroom setting. Further research is needed to better understand the potential influence of these attributes, as well as the value of having aids that can be held and

touched by members of a jury [4,5].

4.3. Qualitative comparison of macromorphoscopic trauma features

In this study a qualitative comparison only evaluated macromorphoscopic features, as fine features are not always well-presented on the 3D printed replicas given the resolution of the CT scans used [22]. Nevertheless, the prints are not intended to be used by the forensic specialist to perform analysis and interpretation of fine and microscopic trauma details, the purpose of the prints is for use as demonstrative aids

for use in court, so that the macromorphology can be observed by the jurors to help with their evaluation of the expert witness testimony. The two-3D printed trauma calvaria in this study were considered to sufficiently demonstrate the macromorphology of the trauma wounds. The GST wounds were clearly observable with defined edges, bevelling and the inclusion of fracture lines. The BFT wound was also observable on both the endocranial and ectocranial surfaces of the printed replica, with plastic deformation and macro fracture lines visible. The scaled calvarium print example illustrating the bullet path through the calvarium also effectively demonstrated the pathway between the entry and exit GST wounds in real space. The build supports inside the scaled calvarium could not be removed in this case, as they were holding the printed rod in place. However, to achieve a better-quality replica it may not always be necessary to 3D print the rod in place and instead, any object could be used to demonstrate the bullet path after printing the calvarium alone.

The 3D printed cranium (case 3) did exhibit some issues. While the printed replica resembled the 3D STL model, there were features such as two large radiating fractures from the volume rendering that were missing on the print. This issue stems from the clinical CT parameters used during scanning and the limitations of segmenting PMCT data when soft tissues are still present [14]. Segmentation of the skeletal material presented with the calvaria in cases 1 and 2 was more straightforward than case 3, due to the absence of soft tissues. The effect of the presence of soft tissue on segmentations could be further explored to produce future guidance for use by forensic imaging specialists. The inclusion of metallic artefacts in the PMCT scan of case 3 may also have affected the CT values and complicated the segmentation process. Further, the quality of a print is dependent on the experience of the observer due to the degree of tacit knowledge involved in segmentation [17]; the observer in this study was familiar with segmenting dry bone CT scan data, but less familiar with segmenting bones from a cadaver with soft tissues present. Users must be careful when segmenting hard tissue and always refer back to original renders demonstrating the importance of insuring transparency in the presentation of the modelling process in forensic applications that ensures any limitations are clearly presented and evaluated. To assess the accuracy of the 3D prints to a greater degree, a further assessment could have been performed by scanning the 3D printed models and performing a mesh-to-mesh comparison with the CT scans of the original bones, as recommended by Baier et al. [38]. However, while mesh comparisons allow for more precise measurements of accuracy or mesh deviations, the method is not always effective for identifying morphological differences [23]. In all cases, qualitative comparisons of the 3D print with the CT volume renders are vital for assessing the quality of printed replicas and identifying any errors.

5. Conclusion

This study evaluates the suitability of three 3D printed cranial trauma examples as 3D physical reconstructions. Through the comparison of three samples, it was identified that:

- 1) the printed trauma wounds were adequate representations of the virtual wounds, and potentially offer a useful tool for the representation of bullet wound size
- 2) printed replicas can offer a valuable, tangible tool for demonstrating a bullet path through a cranium exhibiting GST
- 3) GST and BFT were both effectively visualised on the printed dry bone replicas, however there were limitations with modelling of the PMCT data
- 4) The fracture lines on the printed models were less detailed than the original calvaria

This study provides insights into prospective applications of 3D printing for presenting cranial trauma. While the degree of concordance

between 3D prints of trauma features and original 3D models was good, challenges were identified in generating model and prints from CT data with, for example, not all fracture lines being successfully replicated. To provide accurate tangible 3D printed reconstructions for courtroom demonstrations, further research is needed to explore 3D modelling limitations and 3D printing capabilities for a range of trauma cases. Meanwhile, the concurrent use of virtual and printed 3D models remains important for courtroom applications in addition to continuing to assess the best means of ensuring sufficiently accurate representations when using 3D prints for forensic applications.

Funding

This research did not receive any specific grant from funding agencies in the public, commercial, or not-for-profit sectors.

CRedit authorship contribution statement

Rachael Carew: Conceptualization, Data curation, Formal analysis, Methodology, Writing - original draft. **James French:** Supervision, Writing - review & editing. **Ruth M Morgan:** Supervision, Writing - review & editing.

Declaration of Competing Interest

The authors declare that they have no known competing financial interests or personal relationships that could have appeared to influence the work reported in this paper.

Acknowledgements

We express our gratitude to Dr Edda Guareschi from Murdoch University for providing the osteological samples and PMCT data, without whom this study could not have taken place. We also give thanks to observer 2 for giving their time to participate in the study.

References

- [1] Royal Anthropological Institute. Code of Practice for Forensic Anthropology 2018 https://www.therai.org.uk/images/stories/Forensic/Code_of_Practice_for_Forensic_Anthropology.pdf.
- [2] S. Blau, D. Ranson, C. O'Donnell, Introduction, in: S. Blau, D. Ranson, C. O'Donnell (Eds.), *An Atlas of Skeletal Trauma in Medico-Legal Contexts*, Academic Press, 2018, pp. vii–xvii.
- [3] R.M. Carew, D. Errickson, Imaging in forensic science: five years on, *J. Forensic Radio. Imaging* 16 (2019) 24–33, doi: 10.1016/j.jofri.2019.01.002.
- [4] S. Blau, E. Phillips, C. O'Donnell, G. Markowsky, Evaluating the impact of different formats in the presentation of trauma evidence in court: a pilot study, *Aust. J. Forensic Sci.* 51 (6) (2018) 695–704, doi: 10.1080/00450618.2018.1457717.
- [5] D. Errickson, H. Fawcett, T.J.U. Thompson, A. Campbell, The effect of different imaging techniques for the visualisation of evidence in court on jury comprehension, *Int. J. Leg. Med.* 134 (2020) 1451–1455, doi: 10.1007/s00414-019-02221-y.
- [6] R.M. Carew, R.M. Morgan, C. Rando, A preliminary investigation into the accuracy of 3D modeling and 3D printing in forensic anthropology evidence reconstruction, *J. Forensic Sci.* 64 (2) (2019) 342–352, doi: 10.1111/1556-4029.13917.
- [7] R.M. Morgan, Conceptualising forensic science and forensic reconstruction. Part I: a conceptual model, *Sci. Justice* 57 (6) (2017) 455–459, doi: 10.1016/j.scijus.2017.06.002.
- [8] S.A. Symes, N.E. Abbé L, E.N. Chapman, I. Wolff, D.C. Dirkmaat, Interpreting traumatic injury to bone in medicolegal investigations, in: D.C. Dirkmaat (Ed.), *A Companion to Forensic Anthropology*, Blackwell Publishing Ltd, Chichester, 2012, pp. 340–389.
- [9] N. Dempsey, S. Blau, Evaluating the evidentiary value of the analysis of skeletal trauma in forensic research: a review of research and practice, *Forensic Sci. Int* 307 (2020), 110140, <https://doi.org/10.1016/j.forsciint.2020.110140>.
- [10] K. Puentes, F. Taveira, A.J. Madureira, A. Santos, T. Magalhaes, Three-dimensional reconstitution of bullet trajectory in gunshot wounds: a case report, *J. Forensic Leg. Med.* 16 (7) (2009) 407–410, doi: 10.1016/j.jflm.2009.04.003.
- [11] B.J. Henwood, T.S. Oost, S.I. Fairgrieve, Bullet caliber and type categorization from gunshot wounds in *sus scrofa* (Linnaeus) long bone, *J. Forensic Sci.* 64 (4) (2019) 1139–1144, <https://doi.org/10.1111/1556-4029.14004>.

- [12] A.A.S. Marais, H.J. Dicks, Utilization of X-ray computed tomography for the exclusion of a specific caliber and bullet type in a living shooting victim, *J. Forensic Sci.* 64 (1) (2019) 264–269, <https://doi.org/10.1111/1556-4029.13805>.
- [13] R.M. Carew, D. Errickson, An overview of 3D printing in forensic science: the tangible third-dimension, *J. Forensic Sci.* 65 (5) (2020) 1752–1760, <https://doi.org/10.1111/1556-4029.14442>.
- [14] Z. Obertová, A. Leipner, C. Messina, A. Vanzulli, B. Fliss, C. Cattaneo, L. M. Sconfienza, Postmortem imaging of perimortem skeletal trauma, *Forensic Sci. Int.* 302 (2019), 109921, <https://doi.org/10.1016/j.forsciint.2019.109921>.
- [15] A. Brough, G. Rutty, C. Villa, K. Colman, F. Dedouit, S.J. Decker, The benefits of medical imaging and 3D modelling to the field of forensic anthropology: positional statement of the members of the forensic anthropology working group of the International Society of Forensic Radiology and Imaging, *J. Forensic Radiol. Imaging* 18 (2019) 18–19, <https://doi.org/10.1016/j.jofri.2019.07.003>.
- [16] A. Christensen, M. Smith, D. Gleiber, D. Cunningham, D. Wescott, The use of X-ray computed tomography technologies in forensic anthropology, *Forensic Anthropol.* 1 (2) (2018) 124–140, <https://doi.org/10.5744/fa.2018.0013>.
- [17] D. Fleming-Parrell, K. Michailidis, A. Karantanas, N. Roberts, E.F. Kranioti, Virtual assessment of perimortem and postmortem blunt force cranial trauma, *Forensic Sci. Int.* 229 (1–3) (2013) e1–e6, <https://doi.org/10.1016/j.forsciint.2013.03.032>.
- [18] R.M. Carew, M.D. Viner, G. Conlogue, N. Márquez-Grant, S. Beckett, Accuracy of computed radiography in osteometry: a comparison of digital imaging techniques and the effect of magnification, *J. Forensic Radiol. Imaging* 19 (2019), 100348, <https://doi.org/10.1016/j.jofri.2019.100348>.
- [19] W. Baier, J.M. Warnett, M. Payne, M.A. Williams, Introducing 3D printed models as demonstrative evidence at criminal trials, *J. Forensic Sci.* 63 (4) (2018) 1298–1302, <https://doi.org/10.1111/1556-4029.13700>.
- [20] K. Woźniak, E. Rzepecka-Woźniak, A. Moskała, J. Pohl, K. Latacz, B. Dybała, Weapon identification using antemortem computed tomography with virtual 3D and rapid prototype modeling—a report in a case of blunt force head injury, *Forensic Sci. Int.* 222 (1–3) (2012) 29–32, <https://doi.org/10.1016/j.forsciint.2012.06.012>.
- [21] M. Kettner, P. Schmidt, S. Potente, F. Ramsthaler, M. Schrodtt, Reverse engineering—rapid prototyping of the skull in forensic trauma analysis, *J. Forensic Sci.* 56 (4) (2011) 1015–1017, <https://doi.org/10.1111/j.1556-4029.2011.01764.x>.
- [22] R.M. Carew, R.M. Morgan, C. Rando, Experimental assessment of the surface quality of 3D printed bones, *Aust. J. Forensic Sci.* (2020) 1–18, <https://doi.org/10.1080/00450618.2020.1759684>.
- [23] J. Edwards, T. Rogers, The accuracy and applicability of 3D modeling and printing blunt force cranial injuries, *J. Forensic Sci.* 63 (3) (2018) 683–691, <https://doi.org/10.1111/1556-4029.13627>.
- [24] R.H. Grady, L. Reiser, R.J. García, C. Koeu, N. Scurich, Impact of gruesome photographic evidence on legal decisions: a meta-analysis, *Psychiatr. Psychol. Law* 25 (4) (2018) 503–521, <https://doi.org/10.1080/13218719.2018.1440468>.
- [25] D. Errickson, T.J.U. Thompson, B.W.J. Rankin, The application of 3D visualization of osteological trauma for the courtroom: a critical review, *J. Forensic Radiol. Imaging* 2 (3) (2014) 132–137, <https://doi.org/10.1016/j.jofri.2014.04.002>.
- [26] C.A. Barrera, E. Silvestro, J.S. Calle-Toro, P.V. Scribano, J.N. Wood, M.K. Henry, S. Andronikou, Three-dimensional printed models of the rib cage in children with non-accidental injury as an effective visual-aid tool, *Pedia Radio.* 49 (2019) 965–970, <https://doi.org/10.1007/s00247-019-04368-7>.
- [27] G. Jani, A. Johnson, J. Marques, A. Franco, Three-dimensional(3D) printing in forensic science—an emerging technology in India, *Ann. 3D Print. Med.* 1 (2021), 100006, <https://doi.org/10.1016/j.stlm.2021.100006>.
- [28] W. Schweitzer, M. Thali, E. Aldomar, L. Ebert, Overview of the use of 3D printing in forensic medicine, *Rechtsmedizin* 30 (5) (2020) 292–299, <https://doi.org/10.1007/s00194-020-00412-1>.
- [29] W. Baier, D.G. Norman, J.M. Warnett, M. Payne, N.P. Harrison, N.C.A. Hunt, B. A. Burnett, M.A. Williams, Novel application of three-dimensional technologies in a case of dismemberment, *Forensic Sci. Int.* 270 (2017) 139–145, <https://doi.org/10.1016/j.forsciint.2016.11.040>.
- [30] L.C. Ebert, M.J. Thali, S. Ross, Getting in touch—3D printing in forensic imaging, *Forensic Sci. Int.* 211 (1–3) (2011) e1–e6, <https://doi.org/10.1016/j.forsciint.2011.04.022>.
- [31] D.G. Norman, D.G. Watson, B. Burnett, P.M. Fenne, M.A. Williams, The cutting edge - micro-CT for quantitative toolmark analysis of sharp force trauma to bone, *Forensic Sci. Int.* 283 (2018) 156–172, <https://doi.org/10.1016/j.forsciint.2017.12.039>.
- [32] A.J. Collings, K. Brown, Reconstruction and physical fit analysis of fragmented skeletal remains using 3D imaging and printing, *Forensic Sci. Int. Rep.* 2 (2020), 100114, <https://doi.org/10.1016/j.fsr.2020.100114>.
- [33] Slicer Community. 3D Slicer. 4.8.0 ed. Brigham Women’s Hospital, Boston, MA, US.
- [34] A. Fedorov, R. Beichel, J. Kalpathy-Cramer, J. Finet, J.C. Fillion-Robin, S. Pujol, C. Bauer, D. Jennings, F. Fennessy, M. Sonka, J. Buatti, S. Aylward, J.V. Miller, S. Pieper, R. Kikinis, 3D Slicer as an image computing platform for the quantitative imaging network, *Magn. Reson. Imaging* 30 (9) (2012) 1323–1341, <https://doi.org/10.1016/j.mri.2012.05.001>.
- [35] M. Robles, R.M. Carew, R.M. Morgan, C. Rando, A step-by-step method for producing 3D crania models from CT data, *Forensic Imaging* 23 (2020), 200404, <https://doi.org/10.1016/j.fri.2020.200404>.
- [36] Blender Institute. Blender. 2.78 ed. Amsterdam, Netherlands, 2020.
- [37] K.E. Stull, M.L. Tise, Z. Ali, D.R. Fowler, Accuracy and reliability of measurements obtained from computed tomography 3D volume rendered images, *Forensic Sci. Int.* 238 (2014) 133–140, <https://doi.org/10.1016/j.forsciint.2014.03.005>.
- [38] W. Baier, D.G. Norman, M.J. Donnelly, M.A. Williams, Forensic 3D printing from micro-CT for court use- process validation, *Forensic Sci. Int.* 318 (2021), 110560, <https://doi.org/10.1016/j.forsciint.2020.110560>.
- [39] A.L. Brough, J. Bennett, B. Morgan, S. Black, G.N. Rutty, Anthropological measurement of the juvenile clavicle using multi-detector computed tomography—affirming reliability, *J. Forensic Sci.* 58 (4) (2013) 946–951, <https://doi.org/10.1111/1556-4029.12126>.
- [40] C. Villa, K.B. Olsen, S.H. Hansen, Virtual animation of victim-specific 3D models obtained from CT scans for forensic reconstructions: living and dead subjects, *Forensic Sci. Int.* 278 (2017) e27–e33, <https://doi.org/10.1016/j.forsciint.2017.06.033>.